JOURNAL OF CATALYSIS 106, 1–15 (1987)

Acrolein Oxidation over 12-Molybdophosphates

I. Characterization of the Catalyst

J. B. BLACK,* N. J. CLAYDEN,* P. L. GAI,† J. D. SCOTT,‡ E. M. SERWICKA,* AND J. B. GOODENOUGH*

*Inorganic Chemistry Laboratory, University of Oxford, South Parks Road, Oxford OX1 3QR, United Kingdom; †Department of Metallurgy and Science of Materials, University of Oxford, Parks Road, Oxford OX1 3PH, United Kingdom; and ‡I.C.I. PLC Mond Division, The Health, Runcorn Cheshire WA7 4QF, United Kingdom

Received April 17, 1986; revised January 27, 1987

Various compositions x in the catalyst system $K_xH_{3-x}PMo_{12}O_{40} \cdot nH_2O$ have been prepared by conventional techniques and characterized by thermal analysis, X-ray powder diffraction, ^{31}P solid-state NMR, ESR, electron microscopy, ESCA, BET surface-area measurements, and diffuse-reflectance IR spectroscopy. Contrary to common presupposition, no significant solid-solution range was detected. The $x = 3$ (K_3) phase is stable to 920 K; the $x = 0$ (K_0) phases lose their n water of crystallization by 450 K and their constitutional water in the temperature interval $500 < T < 700$ K. Decomposition of the Keggin anion $(PMo_{12}O_{40})^{3-}$ of the $H_3PMo_{12}O_{40} \cdot nH_2O$ phase accompanies the loss of constitutional water, and an identifiable decomposition product is MoO_3. Under normal calcining conditions (673 K in air for 1–5 h), the degree of decomposition of the K_0 phase decreases with increasing x, little MoO_3 being detectable for $x \geq 2$. An epitaxial, isostructural surface layer derived from the $H_3PMo_{12}O_{40} \cdot nH_2O$ appears to be stabilized on the water-insoluble $K_3PMo_{12}O_{40}$ particles. Calcined catalysts in the compositional range $2 < x \leq 3$ consist of well-formed, spherical particles having surface Keggin anions; these catalysts are particularly suitable for mechanistic studies of catalytic reactions on a Keggin unit.

INTRODUCTION

Attempts to use heteropolyacids and their salts as catalysts started in the early sixties, and research in this field has developed rapidly in the last decade. Of particular industrial importance is the catalytic oxidation of acrolein and methacrolein to their corresponding acids by heteropoly-compounds (*1*).

Patent data and literature reports suggest that the catalytic agent for this oxidation reaction is a heteropolyanion with the Keggin structure, and principally the 12-molybdophosphate anion $(PMo_{12}O_{40})^{3-}$ illustrated in Fig. 1. Compounds containing these Keggin anions are particularly suitable for a mechanistic study for at least three reasons: (1) the Keggin unit is the best characterized heteropolyanion, details of the $(PMo_{12}O_{40})^{3}$ anion structure being available from single-crystal data (*2*, *3*); (2) the multifunctional capabilities of 12-molybdophosphoric acid and its salts range from properties associated with Brønsted acidity, such as fast proton conduction (*4*), to those connected with the oxidizing power of individual anions (*5*); (3) as shown in this paper, catalytic particles having surface Keggin units can be prepared; these units provide a microsurface of known structure on which the chemical reaction occurs.

Earlier studies have shown that the protons of the acid form may be substituted by alkali-metal cations M^+; the larger cations K^+, Rb^+, Cs^+, and NH_4^+ form insoluble salts, e.g., $K_3PMo_{12}O_{40}$, whereas the smaller cations Li^+ and Na^+ form hydrated, water-soluble salts (*6*, *7*). Several studies have examined the changes in catalytic properties with composition in mixed sys-

0021-9517/87 $3.00

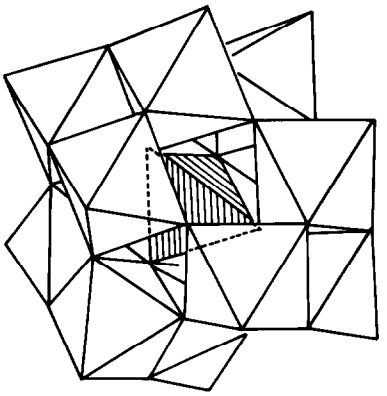

FIG. 1. Structure of the Keggin anion $(PMo_{12}O_{40})^{3-}$. The central PO_4 tetrahedron is shaded; MoO_6 octahedra are unshaded.

tems of formal starting composition $M_xH_{3-x}PMo_{12}O_{40} \cdot nH_2O$; the most satisfactory results have been obtained with the catalysts containing an insoluble salt component $M_3PMo_{12}O_{40}$ (*7–9*). In these studies little characterisation of the catalyst was attempted, and it has generally been assumed that the catalysts form solid-solution pseudobinary systems $M_x(H_3O)_{3-x}PMo_{12}O_{40} \cdot nH_2O$. However, the variations with x of the catalytic performance are difficult to rationalize with such a model, and there is an evident need for a systematic characterization of these catalysts under reactor conditions in order to interpret the selectivity/activity data presented in Part II, which immediately follows this paper. Such a characterization also proves to be an essential preliminary step for the mechanistic studies presented in Part III of this present collected group of papers.

In this paper (Part I) we present a detailed characterization, before and after calcination, of catalysts having the formal composition (as freshly prepared) of $K_xH_{3-x}PMo_{12}O_{40} \cdot nH_2O$. In each of Parts I, II, and III the various samples studied are referred to by the notation K_x, even after subsequent treatment has removed sufficient water to partially decompose the Keggin unit or has reduced this unit and/or introduced into it oxygen vacancies. In this paper we disprove any pseudobinary hypothesis; we show that standard catalyst calcination prior to use may remove more water than the n moles of compositional H_2O of the formal formula, thereby causing reversible and/or irreversible decomposition of Keggin units; we also establish that compositions with $2.5 \leq x \leq 3$ consist, after a standard calcination, of well-formed, spherical K_3 particles having a K_0 ($x = 0$) phase stabilized at their surface with intact Keggin structures.

EXPERIMENTAL

Materials

The catalysts from the K_x series were prepared by the method of Tsigdinos (*10*) according to previously described procedures (*6, 7, 11*). Stoichiometric quantities of $H_3PMo_{12}O_{40} \cdot 24H_2O$ (e.x., BDH Ltd., "AnalaR" grade; exact water content determined by TGA for each batch) and of K_2CO_3 (e.x., BDH Ltd., "AnalaR" grade) were each dissolved in the minimum quantity of water, and the solutions were mixed with stirring. The final product was obtained by evaporation to dryness on a rotary evaporator at 333–353 K under reduced pressure. Subsequently the catalysts were calcined for 5 h in air at 673 K. Compositions $x = 0, 0.5, 1, 1.5, 2, 2.5, 2.75$, and 3 were prepared and examined.

Techniques

(*1*) *X-ray diffraction.* Powder X-ray diffraction data were obtained with a Philips PW-1720 diffractometer and a Guinier-Haag focusing camera. Lattice parameters were refined with the program CELL; powder patterns were simulated from known crystal structures with the program LAZY. Both programs were available on the Oxford University VAXI computer.

(*2*) *Nuclear magnetic resonance.* A Bruker CXP 200 spectrometer operating at 80.9 MHz was used to acquire ^{31}P solid-state NMR spectra. Magic-angle spinning

in Delrin rotors at 4 kHz was employed, and all spectra were referenced externally to 85% orthophosphoric acid.

(*3*) *Thermal analysis*. Thermogravimetric analysis was carried out in static air in a Stanton-Redcroft STA-780 thermal analyser. Samples of around 150 mg (TGA only) or 15 mg (simultaneous TGA/DTA) were heated at 10 K per minute up to 873 K.

(*4*) *Electron-spin resonance*. ESR spectra were recorded at room temperature and at 77 K with a Varian E-112 Century-line spectrometer equipped with a fieldial and operating in the *X* band. DPPH ($g = 2.0036$) was used as a standard for the determination of g factors. Spin densities were estimated with respect to a $VOSO_4$ standard.

(*5*) *Electron microscopy*. Microstructural characterization was carried out with a combination of high resolution (~2 Å) transmission EM (HREM), analytical EM (AEM) for small-area compositional analysis, and scanning EM (SEM) for surface topography of the microcrystals. For transmission EM (TEM) a JEOL JEM 200 CX HREM operating at 200 keV was used; it was fitted with a low-light-level TV camera to facilitate study at very low beam currents of the beam-sensitive crystals. AEM/SEM were carried out with a JEOL JEM 100C Temscan instrument operating at 100 and 20 keV. The samples were suspended in chloroform and supported on copper grids with a holey-carbon-film support.

(*6*) *Infrared spectroscopy*. Diffuse-reflectance IR spectra were acquired on a Nicolet 2000 FTIR spectrometer operating with a diffuse-reflectance cell attachment and made available by I.C.I. PLC (Wilton). Spectra were recorded at 4 cm^{-1} resolution; typically 1000 scans were taken.

(*7*) *Electron spectroscopy for chemical analysis*. ESCA measurements were carried out with an ESCALAB-5 spectrometer (V.G. Scientific); the K_α line of Mg was used as a source of X-ray excitation.

RESULTS

A. Uncalcined Catalysts

(*1*) *X-ray diffraction*. The presence of more than one phase in freshly prepared catalysts was initially detected by X-ray diffraction.

The free acid $H_3PMo_{12}O_{40} \cdot nH_2O$ (denoted as K_0) is very soluble and crystallizes with variable amounts of water of crystallization ($0 \leq n \leq 30$). Samples of the acid used in this work were certainly not single-phase materials. Figure 2a shows the X-ray spectrum of a typical batch of K_0 (e.x., BDH). For comparison, spectra of K_0 with various degrees of hydration prepared under controlled partial pressures of H_2O are presented together with patterns syn-

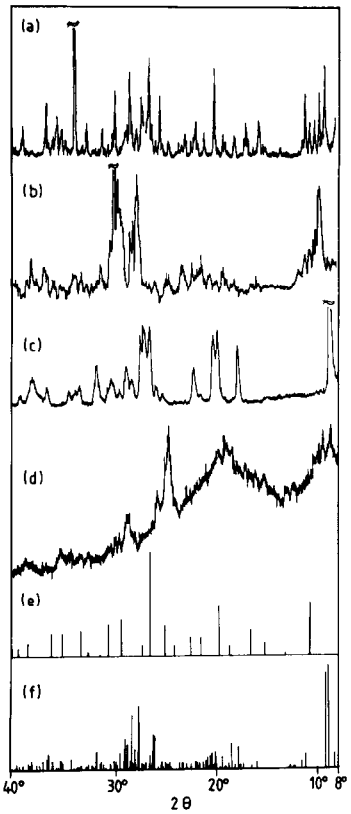

FIG. 2. Powder X-ray diffraction patterns of $H_3PMo_{12}O_{40} \cdot nH_2O$ with various degrees of hydration: (a) typical batch of, e.x., BDH product, $n = 24$; (b) $n = 30$; (c) $n = 8$; (d) $n = 0.2$; (e) $n = 30$, synthesized (2); (f) $n = 13$, synthesized (3).

thesized from the known crystal structures for K_0 with $n = 13$ and $n = 30$ (*2, 3*).

The least-hydrated sample appears almost amorphous to X-rays (Fig. 2d). All the other patterns contain evidence of more than one crystalline phase. While some of the peaks predicted for $n = 13$ and $n = 30$ can be located in the experimental spectrum, it is clear that other phases are present as well. The only experimental spectra of polycrystalline $H_3PMo_{12}O_{40} \cdot nH_2O$ reported in the literature (*12*) do not agree closely with any of the spectra reported here and are unindexed. Thus it is clear that samples of the free acid contain many different phases, as well as an amorphous material, depending on the degree and homogeneity of hydration.

The other end member of the K_x series, K_3, was found to be a single-phase material with good crystallinity. The X-ray powder pattern of this catalyst (Fig. 3) corresponds exactly to that synthesized from the reported crystal structure of K_3 (*13*).

Diffraction patterns of samples with intermediate composition ($0.5 \leq x \leq 2.0$) demonstrate the existence of more than one crystalline phase. All traces contain the lines characteristic of K_3, but comparison of the patterns of K_1 (Fig. 4) and K_3 (Fig. 3) shows that these lines become less intense as x falls. The additional peaks in Fig. 4 agree exactly with the principal peaks found for the $K_0 \cdot 8H_2O$ sample (Fig. 2). In other preparations peaks corresponding to other free acid phases were also observed. The $K_0 \cdot 8H_2O$ peaks were also detected in decreasing intensity with increasing x for other samples with $x < 2$. The X-ray data for $2 \leq x \leq 3$ revealed only the K_3 phase.

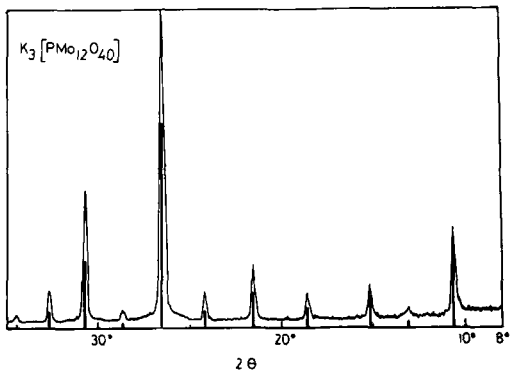

FIG. 3. Powder X-ray diffraction pattern of K_3, experimental and synthesized (*13*).

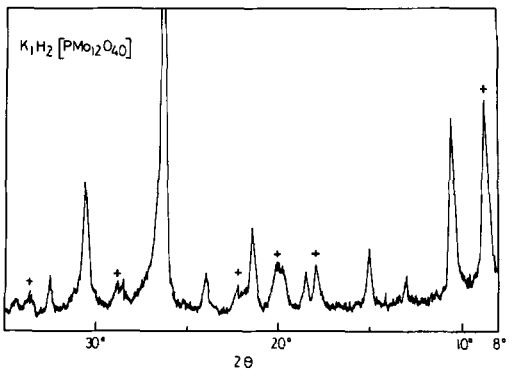

FIG. 4. Powder X-ray diffraction pattern of K_1. Peaks corresponding to K_0 phases are marked with a cross.

Refinement of the lattice parameter of the phase with K_3 structure was accomplished with a standard set of 15 reflections observed for all samples. Variation of this lattice parameter with x could provide evidence for a solid-solution region. However, the data show no significant change in unit-cell size, although there is a large increase in experimental error as the K_3 pattern becomes less intense.

(*2*) *^{31}P solid-state NMR.* A ^{31}P solid-state NMR study was undertaken in order to gain further insight into the multiphase nature of the K_x series. The spectra of fresh catalysts ($1 \leq x \leq 3$) are shown in Fig. 5. All samples except K_3 show the presence of more than one phosphorus resonance, which confirms the conclusion from the X-ray data that, for $x < 3$, the structures are complex. The K_3 sample shows a single, sharp resonance at $\sigma = -4.3$ ppm, which indicates a uniform phosphorus environment in this catalyst. The peak characteristic of K_3 appears also in the spectra of all the other potassium-containing members of the series, which demonstrates the presence of a neutral salt in agreement with the X-ray data. The

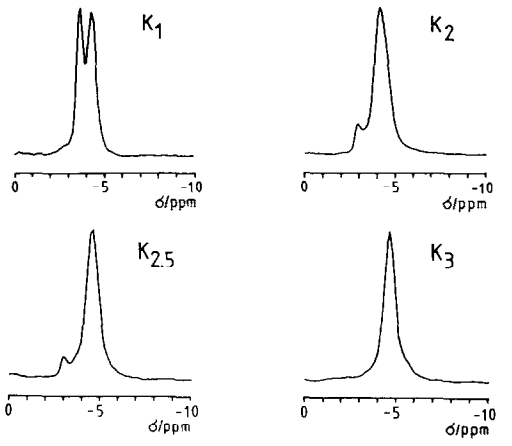

FIG. 5. ^{31}P solid-state NMR spectra of uncalcined K_x catalysts.

appearance of other peaks is attributed to the occurrence of the K_0 phase with an inhomogeneous water content.

In a separate experiment it was found that K_0 gives several resonances which vary with the amount of water of crystallization. For instance, the K_0 hydrates with $n = 30$ and $n = 8$ give resonances at $\sigma = -3.9$ and -3.6 ppm, respectively, whereas samples with little or no water of crystallization show peaks at $\sigma = -2.0$ and -2.9 ppm. For this reason, absorption at $\sigma = -3.7$ ppm in the spectrum of K_1 and a peak at $\sigma = -3.0$ ppm present in K_2 and $K_{2.5}$ are assigned to K_0 phases having different degrees of hydration.

It was found that the spectra of fresh catalysts showed better resolution when samples were stored in a wet atmosphere (330 K, 150 Torr H_2O).[1] This is consistent with the observation that the K_0-phase composition is very sensitive to the H_2O partial pressure. When stored in air, it tends to produce a number of different hydrates as well as amorphous material, which results in a variety of phosphorus environments and, consequently, a broadening of the ^{31}P resonance.

(3) Thermogravimetric analysis. Further evidence that there is no solid-solution range for any value of x comes from the TGA traces of the catalysts. Two types of water loss can be distinguished: the water of crystallization (nH_2O) and the constitutional water (1.5 H_2O for $H_3PMo_{12}O_{40} \cdot nH_2O$). The only feature of the TGA curve for fresh K_3 (Fig. 6a) is the loss of physisorbed water below 500 K; otherwise, it is thermally stable up to 920 K. On the other hand, the K_0 sample (Fig. 6b) loses its water of crystallization by 450 K, and the weight loss observed in the range 500–700 K corresponds exactly to the weight loss expected on complete decomposition of the acid (1.5 water molecules per Keggin anion). TGA profiles for the catalysts with intermediate values of x up to $x = 2.75$ were obtained, and all samples behaved as mixtures of the end members, K_0 and K_3, of the series. The curve for $K_{2.5}$ is presented as an example in Fig. 6c. In particular, the weight loss between 500 and 700 K was consistent with the formulation $(x/3)K_3PMo_{12}O_{40} + [(3 - x)/3]H_3PMo_{12}O_{40}$, but not with the solid-solution stoichiometry $(M^+)_x(H_3O^+)_{(3-x)}(PMo_{12}O_{40})^{3-}$. In addition, the features observed in the DTA curve for K_0 are reproduced throughout the entire composition range for $x \leq 2.75$.

Finally, it is significant that the weight change due to the loss of constitutional water from the K_0 component in the samples with $x \geq 2.5$ ends at temperatures higher by ca. 20 K than for the rest of the series, indicating that the K_0 phase is more stable against calcination temperatures at these higher x values.

B. Calcined Catalysts

(1) Calcination. Industrial catalysts are usually calcined at temperatures higher than the operating temperature in the reactor. This procedure is to ensure that the catalyst will be thermally stable in the reactor and to eliminate possible structural degradation due to sintering effects. Any changes with time in the catalytic properties can then be attributed to the influence of the reagents on the catalyst structure.

[1] 1 Torr = 133 Pa.

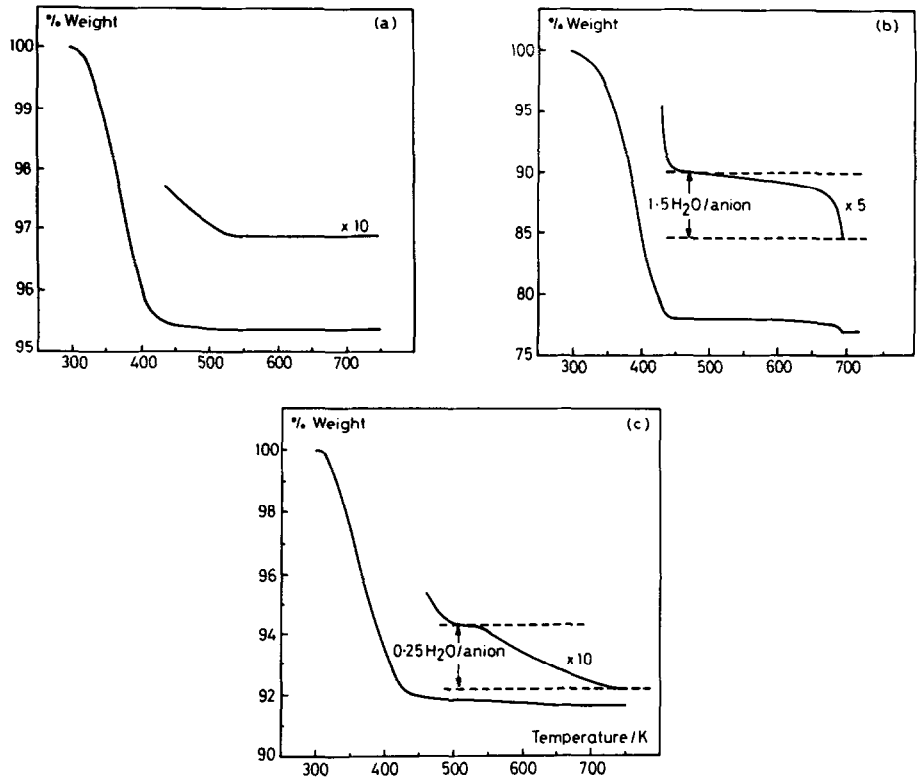

FIG. 6. TGA curves of (a) K_3, (b) K_0, (c) $K_{2.5}$.

In acrolein and methacrolein oxidation, polymolybdophosphate catalysts generally operate at around 573–623 K after calcination at 623–673 K. In this study, calcination was carried out at 673 K for 5 h in static air, and the catalytic operating temperature was 623 K.

From the TGA data it is known that the K_3 component of the catalyst is thermally stable up to 920 K. However, examination of the TGA curve for K_0 (Fig. 6b) shows that all water of crystallization is lost below 500 K, and the rate of loss of constitutional water is significant at 623 K. Thus calcination may lead to partial or total decomposition of some of the K_0 component in the catalyst and, consequently, to an even more complex phase composition of the working catalyst.

In order to elucidate this point further, the effects of calcination on fresh catalysts were investigated by ^{31}P solid-state NMR, X-ray diffraction, ESR, and electron microscopy.

(2) ^{31}P solid-state NMR. The spectra were recorded after varying times of calcination ranging from 15 min to 15 h. After each stage, the calcined samples were subjected to steaming at 330 K in order to identify the reversible changes due to the loss of water.

Neither prolonged calcination nor subsequent steaming alter the ^{31}P NMR spectra of the K_3 sample. The single resonance at $\sigma = -4.3$ ppm remains the only feature of all K_3 spectra, again proving this phase to be a stable component of the K_x catalysts studied.

In contrast, all K_x samples of intermediate composition ($1 \leq x \leq 2.5$) show clear evidence of a component that varies with calcination conditions. Figure 7 (continuous line) presents the spectra of samples calcined for 1 h. All contain the resonance

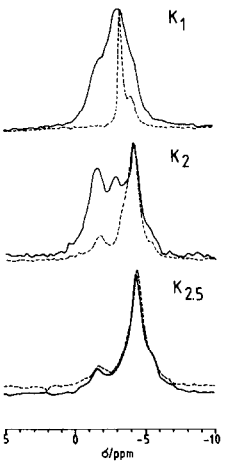

FIG. 7. ^{31}P solid-state NMR spectra of the K_x catalysts calcined for 1 h at 673 K (continuous line) and steamed at 330 K (dashed line).

at $\sigma = -4.3$ ppm characteristic of the K_3 phase as well as a number of other resonances. Broad peaks at $\sigma = -1.7$ and -3.0 ppm dominate the spectrum of the K_1 sample. They are also a prominent feature of the K_2 spectrum. For the $K_{2.5}$ catalyst, only the $\sigma = -1.7$ resonance can be clearly distinguished. Both resonances fall in the range observed for partially dehydrated K_0 (see paragraph A.2). Subsequent steaming tends to reverse the effects of calcination on K_1 and K_2 samples (Fig. 7, dashed line), almost restoring their initial spectra. The reversibility of changes observed in the NMR spectra upon steaming is consistent with the assumption that the new peaks are due to phases of the free-acid component that had suffered loss of water, but had not yet undergone an irreversible decomposition.

This assumption was tested further. The TGA curve of a sample of K_1 immediately after calcination for 5 h at 673 K showed a weight loss in the region 500–700 K equivalent to 0.7 molecules of water per anion compared to 1 molecule per anion for the fresh catalyst. This indicates that no more than 30% of the Keggin units in the K_0 component of K_1 had decomposed with loss of constitutional water. Therefore the majority of the Keggin units of the K_1 sample remain undecomposed, and the strong resonances at $\sigma = -1.7$ and -3.0 ppm may be associated with phases containing the complete Keggin unit with no oxygen loss.

Surprisingly, the spectrum of calcined $K_{2.5}$ is practically not affected by steaming. The persistence of the $\sigma = -1.7$ ppm resonance in this sample and in K_2 after steaming indicates that for some reason an anhydrous K_0 present behaves differently in the K_3-rich sample than in catalysts rich in the K_0 phase. Moreover, the disappearance of the $\sigma = -3.0$ ppm resonance suggests that the resonance associated with K_0 at a K_3 interface may be distinguished from the part of the K_0 phase distant from this interface.

A study of the catalyst behavior upon prolonged exposures to calcination conditions brings a further indication that the properties of the K_0 component in $K_{2.5}$ are special. The NMR spectra of K_1 and K_2 show stepwise degradation of the K_0 phase. The evolution of the NMR spectra of K_2 with time of calcination is shown in Fig. 8 (continuous line) together with the effect of steaming (dashed line). Prolonged treat-

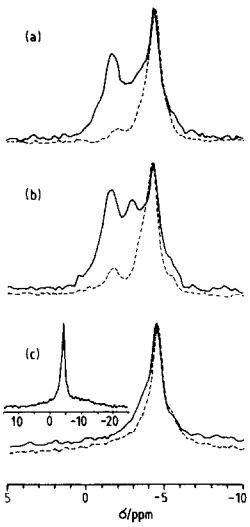

FIG. 8. ^{31}P solid-state NMR spectra of the K_2 catalyst calcined at 673 K for different periods of time (continuous line) and steamed at 330 K (dashed line): (a) 15 min, (b) 1 h, and (c) 15 h.

ment is seen to lead to the irreversible disappearance of distinct peaks, eventually including that at $\sigma = -1.7$ ppm, associated with the dehydrated K_0. They are replaced by a broad envelope (background to the $\sigma = -4.3$ ppm peak of K_3) of numerous ^{31}P resonances centered around $\sigma = -8$ ppm (not easily discernible in Fig. 8c); this envelope is obviously due to the products of thermal decomposition of the K_0 phase. On the other hand, the NMR spectrum of $K_{2.5}$ did not change substantially upon prolonged calcination. The peak at $\sigma = -1.7$ ppm could still be detected even after 15 h treatment, indicating that the K_0 component in $K_{2.5}$ must indeed become stabilized against thermal decomposition at 673 K.

(*3*) *X-ray diffraction.* The NMR experiments clearly show gradual decomposition of the K_0 phase. This process may occur through a number of intermediate steps before the final formation of mixed molybdenum and phosphorus oxide phases. Powder X-ray diffraction was employed in an attempt to identify the new phases present in the calcined catalysts.

Samples of the K_x series were investigated after calcination at 673 K for 5 and 24 h. The K_3 component of the X-ray patterns remained unchanged even after prolonged calcination. In all samples with $x \leq 2.5$, lines due to MoO_3 could be detected (as reported by Konishi *et al.* (*12*)) after calcination for 24 h, but the intensity of the peaks decreased with increasing x until, for $x = 2.5$, only a very small peak corresponding to the most intense line of MoO_3 was found. After calcination for 5 h, MoO_3 lines were found in the X-ray patterns only for the compositions $x \leq 1.5$; Fig. 9 shows the trace for $x = 1.5$.

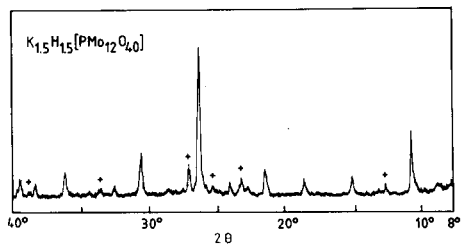

FIG. 9. Powder X-ray diffraction pattern of $K_{1.5}$ calcined for 5 h at 673 K. Peaks corresponding to MoO_3 are marked.

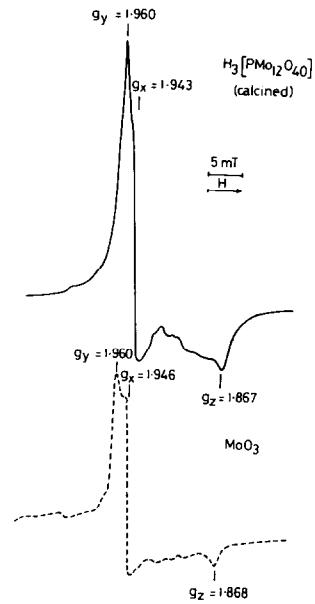

FIG. 10. ESR spectra of K_0 calcined at 673 K (continuous line) and slightly reduced MoO_3 (dashed line). Spectra recorded at 77 K.

(*4*) *Electron-spin resonance.* ESR experiments provided additional evidence for the presence of MoO_3 in catalysts of the K_x series after calcination at 673 K for 5 h. Figure 10 shows the ESR signal obtained for a sample of calcined K_0 and, for comparison, the ESR signal of MoO_3 after slight reduction by high-temperature evacuation. The latter spectrum has been shown (*14*) to arise from an unpaired electron localized at a coordinatively unsaturated molybdenum center of C_{2v} symmetry. This symmetry corresponds to loss of a bridging oxygen atom *trans* to the short Mo=O molybdenyl bond in MoO_3. Identical lineshapes and ESR parameters for calcined K_0 show that this signal can be assigned to the MoO_3 phase formed by decomposition of some Keggin units.

The presence of any ESR signal requires a degree of reduction of the MoO_3 formed

and is not, therefore, a quantitative measure of the MoO_3 present. In fact, the signal from the calcined K_0 corresponded to a reduction of only 0.02% of the total molybdenum present in the sample. Nevertheless, this signal was observed for all samples with $x \leq 2.5$, although its intensity decreased with increasing x. This observation confirms the presence of an MoO_3 component in all calcined catalysts of composition $x \leq 2.5$.

(5) *Electron microscopy.* Transmission electron microscopy and scanning electron microscopy (TEM and SEM) of the calcined catalysts were undertaken in order to obtain a better picture of the catalyst morphology and the distribution of the products of the K_0-phase decomposition.

As shown in Figs. 11a and 11b, the K_3 and $K_{2.5}$ samples are composed of well-formed, round and hexagonal crystallites 1–3 μm in diameter for K_3 and 0.5–1 μm for $K_{2.5}$; they give electron-diffraction patterns characteristic of cubic K_3 (Fig. 11c). SEM images of the surface topography of the microcrystals in $K_{2.5}$ (Fig. 11d) show them to be defect-free, clean single crystallites. Only one MoO_3 microcrystal was detected in the entire $K_{2.5}$ sample examined with electron diffraction and AEM; in agreement with the ESR result, this observation shows that some decomposition of the K_0 component does occur in the $K_{2.5}$ sample.

In contrast, samples rich in the K_0 phase, such as K_1 shown in Fig. 12, consist of

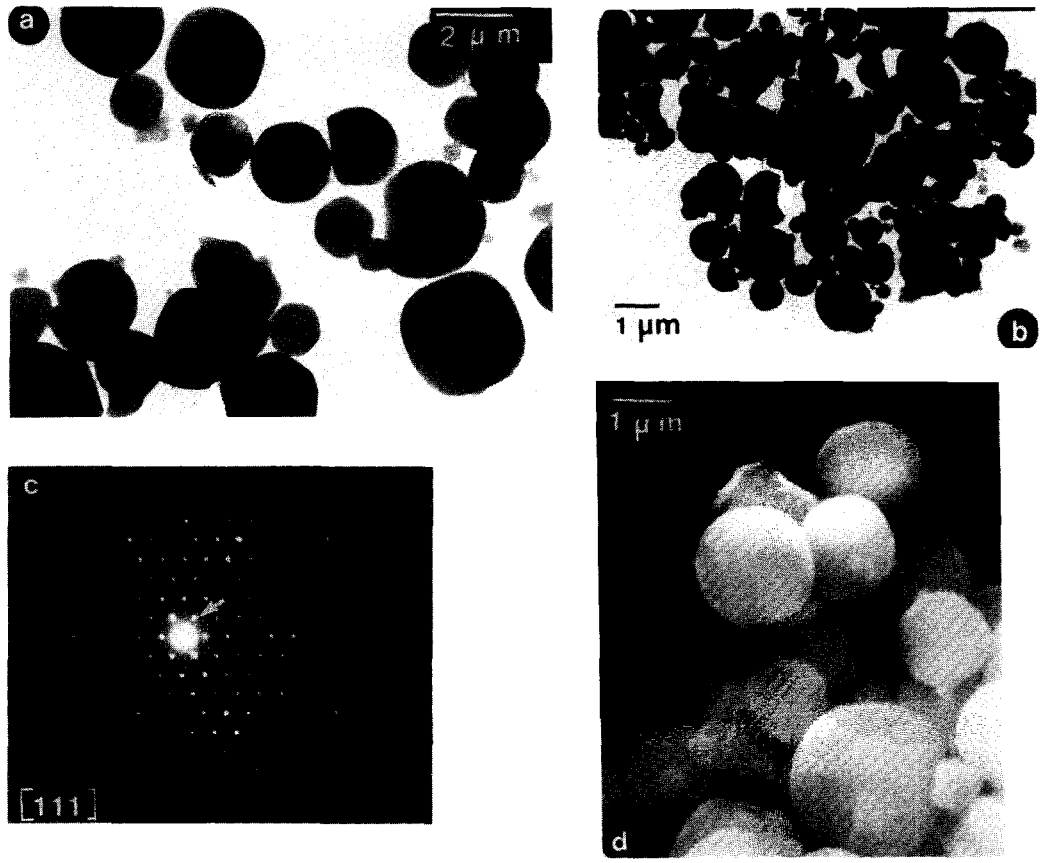

FIG. 11. TEM morphology of calcined (673 K) samples, (a) K_3 and (b) $K_{2.5}$; (c) [111] electron-diffraction pattern of cubic K_3 with (110) reflections (e.g., arrow), d spacing $\cong 8.2 \pm 0.1$ Å; and (d) SEM image of calcined $K_{2.5}$.

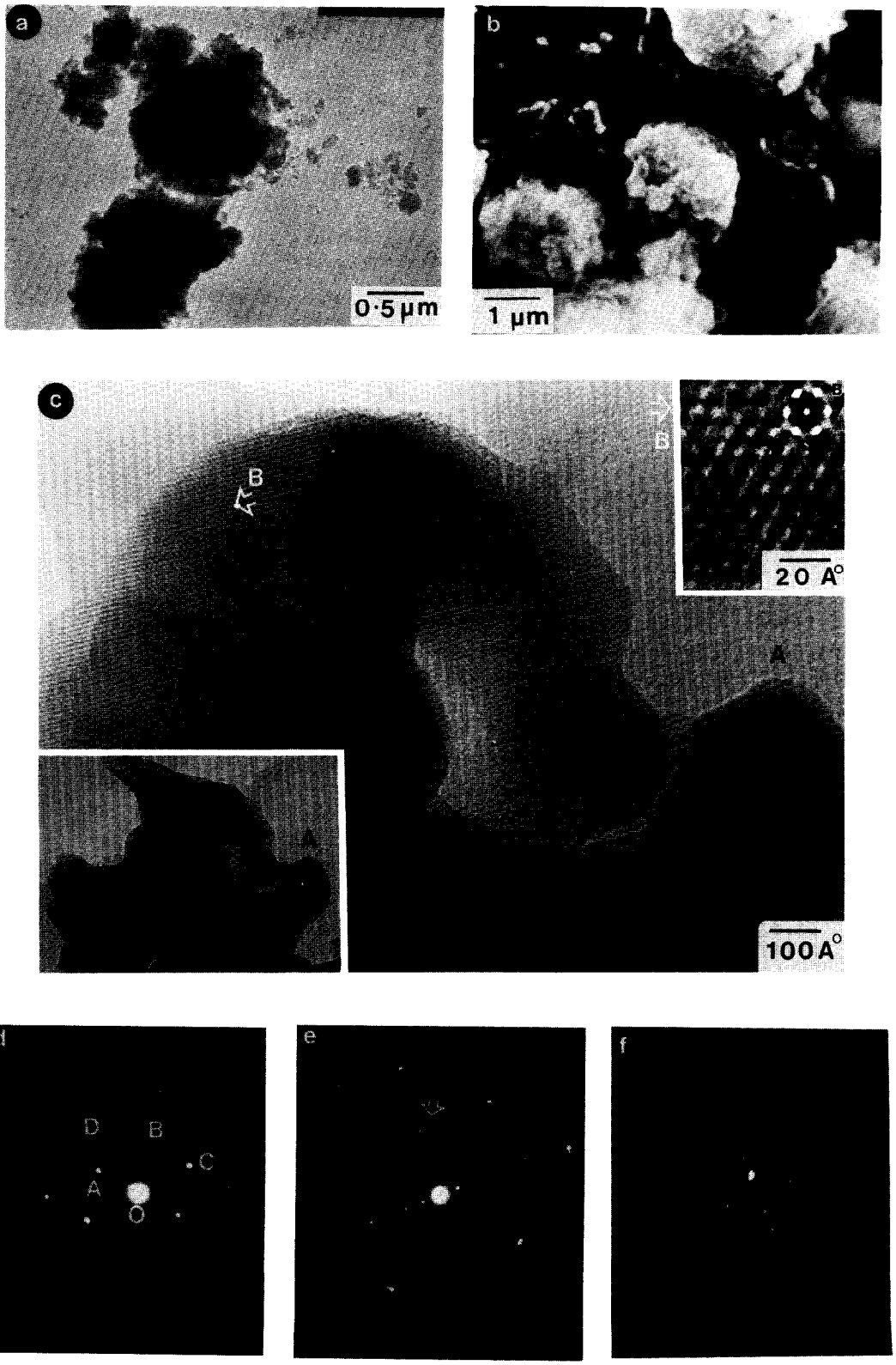
a
0·5 μm
b
1 μm
c
B
B
20 A°
A
A
100 A°
d
D
B
C
A
O
e
f

agglomerates of poorly crystalline material and represent a mixture of several phases, namely K_3, MoO_3, and some unidentified phases that could not be indexed, but are likely to be formed during the decomposition of K_0. In several diffraction patterns the Bragg spots were streaked, indicating considerable disorder in the crystals. The TEM morphology of K_1 is shown in Fig. 12a. The SEM image of Fig. 12b reveals a surface topography consisting of agglomerates of microcrystals with rough surfaces. Interpenetrating microcrystals in K_1 are clearly seen in the HREM image of Fig. 12c, which illustrates orientation relationships of the [111] zones of the crystallites. The multiphase nature of the K_1 sample is demonstrated by the set of electron-diffraction patterns shown in Figs. 12d, 12e, and 12f; they represent, respectively, a recurring intermediate "monoclinic" phase, an "orthorhombic" phase superimposed on the [111] zone of K_3, and the [111] zone of K_3. Crystallites of K_3 in these samples were found to be of much smaller size than those found in the sample of pure K_3; the presence of a significant concentration of K_0 apparently inhibits sintering of the K_3 phase during calcination. A rough estimate showed that the MoO_3 present made up about 5–10% of the K_1 sample. This is just above the level at which it can be detected by standard X-ray diffraction methods.

A particularly valuable piece of information was obtained from the study of the calcined K_0 sample. As shown in Fig. 13a, calcined K_0 consists of irregularly shaped agglomerates of microcrystals. A considerable amount of MoO_3 was detected, as expected; the morphology of a MoO_3 needle with (010) habit and its diffraction pattern are shown in Fig. 13b. Significantly, the selected-area diffraction patterns from individual microcrystals of the sample have shown that some of the calcined K_0 forms a phase that is isostructural with K_3, as is demonstrated in the diffraction pattern in Fig. 13c. The rings correspond to the reflections in the [111] zone of K_0 with *d* spacings identical to those of the [111] zone of K_3. The superimposed spots in Fig. 13c show a "monoclinic" orientation that is similar to the one observed in K_1 (Fig. 12d); it is presumably due to one of the intermediate decomposition products of K_0.

Identification of the isostructural relationship between K_3 and one of the dehydrated K_0 phases provides direct evidence in support of our deduction that an epitaxial growth of a stabilized K_0 layer occurs on the surface of K_3 crystallites during calcination. The isostructural relationship between the two phases could facilitate proton transfer across the interface, thus enhancing the thermal stability of the surface layer formed. The presence of an isostructural, epitaxial layer would not affect the diffraction pattern of the K_3 matrix, and indeed the electron diffraction patterns of the $K_{2.5}$ sample bear no evidence of streaking.

C. Catalyst Surface

Surface vs bulk properties. The techniques described above give information about the several phases present throughout the bulk of a catalyst, but they provide only indirect evidence about the character of the surface of the particles. Heterogeneous catalysis occurs at the catalyst surface, and the surface structure of a solid can differ greatly from that of the bulk.

FIG. 12. Microstructure of calcined (673 K) K_1. (a) TEM morphology, (b) SEM image, (c) HREM image in [111] projection showing single-crystal character of individual, interpenetrating microcrystals (inset A) and comparison of the image with calculations for $\cong$100 Å thick crystal (inset B); selected-area electron-diffraction patterns of intermediate (d) monoclinic (OB $\cong$ 3.1 $\pm$ 0.1 Å, OA $\cong$ 3.4 $\pm$ 0.1 Å, $\sphericalangle$ AOB $\cong$ 77 $\pm$ 2°, $\sphericalangle$ DOC $\cong$ 84 $\pm$ 2°), (e) orthorhombic (dimensions: $\cong$2.0 $\pm$ 0.1 Å and $\cong$2.5 $\pm$ 0.1 Å) superimposed on [111] K_3, and (f) [111] K_3 phases present in K_1.

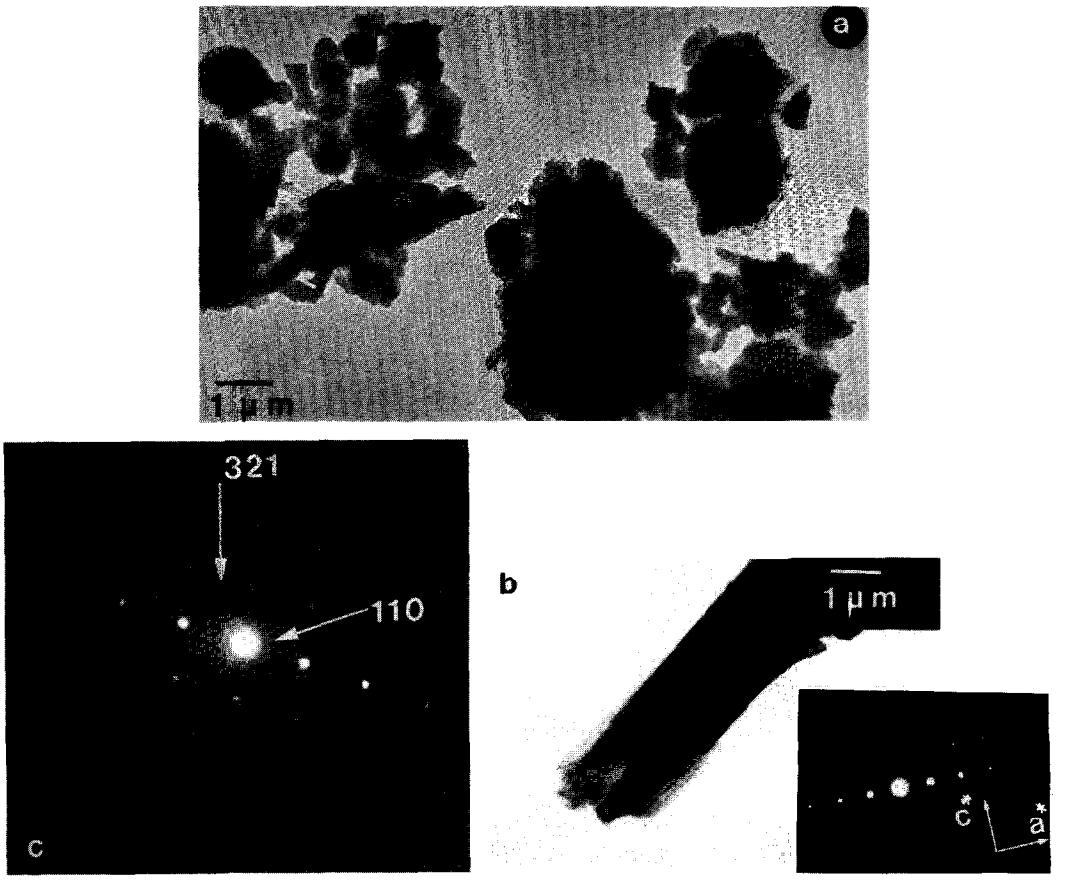

FIG. 13. Microstructure of calcined (673 K) K_0. (a) TEM morphology, (b) embedded (010) MoO_3 platelet and corresponding electron-diffraction pattern, and (c) electron-diffraction pattern showing faint rings of (110) and (321) reflections (d spacings = 8.2 ± 0.1 and 3.1 ± 0.1 Å, respectively) of phase isostructural with K_3.

In the present study we have presented evidence for the possibility of a "surface coat" of the soluble K_0 component on crystallites of the insoluble K_3. In light of the thermal instability of the K_0 phase, it becomes essential to confirm that the intact Keggin anions are present at the catalyst surface after calcination.

(*1*) *BET surface-area measurements.* Figure 14 shows the variation of surface area of the calcined catalysts with potassium content. The free acid has low surface area (2.5 $m^2\ g^{-1}$) while the surface area of the neutral potassium salt is an order of magnitude higher (33.0 $m^2\ g^{-1}$). The variation in surface area with potassium content shows a rapid fall as some of the K_0 component is introduced. Since the K_3 crystallites are largest in the K_3 sample, this observation apparently means that K_0 must

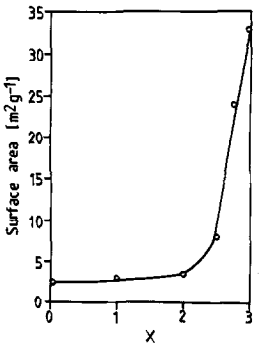

FIG. 14. Effect of catalyst composition on the BET specific surface area of calcined (673 K) catalysts.

block micropores in the K_3 crystallites that contribute to the BET surface area (*15*) as well as causing the agglomeration of these crystallites. The occurrence of agglomeration has been demonstrated in Fig. 12.

(*2*) *Electron spectroscopy for chemical analysis*. Coating of K_3 crystallites by a K_0 phase should lead to a potassium deficiency at the catalyst surface compared to the bulk. This possibility was investigated by carrying out a chemical analysis of the surface of calcined catalysts by X-ray photoelectron spectroscopy. Wide scans were carried out on each sample to confirm the presence of all the elements expected and the absence of impurities; narrow scans were subsequently taken for each element analyzed. The results, shown in Table 1, demonstrate that there is indeed a significant potassium deficiency for all samples with $x < 3$.

(*3*) *Diffuse-reflectance infrared spectroscopy*. In view of the thermal instability of the K_0 component, it is important to establish as far as possible that the Keggin unit is indeed responsible for the catalytic properties of these catalysts.

Information from the catalyst surface is strongly enhanced by using IR spectroscopy in the diffuse-reflectance mode. Spectra of the calcined K_x series obtained in this mode show predominantly the presence of the Keggin unit. Figure 15 shows, as an example, the spectrum of K_1 in the region 1200–500 cm^{-1}. The four strong bands at 1060, 970, 870, and 790 cm^{-1} are characteristic of the Keggin unit (*16*). Additionally, a small shoulder around 990 cm^{-1}, which is the frequency of the M=O double-bond stretch in MoO_3, could be detected. No bands characteristic of MoO_3 were observed for higher values of x. This result shows that, although the presence of MoO_3 for compositions $x \leq 2.5$ has been demonstrated by other techniques, it does not contribute substantially, even at low values of x, to the exposed surface area, where the principal species is seen to be the undecomposed Keggin unit.

TABLE 1

Surface Analysis of the K_x Series

Sample	Elemental ratios		
	K	P	Mo
K_1	0.3 ± 0.2	1.3 ± 0.5	12
K_2	0.7 ± 0.2	1.2 ± 0.5	12
$K_{2.5}$	1.6 ± 0.2	1.4 ± 0.5	12
K_3	3.0 ± 0.2	1.3 + 0.5	12

Note. All analyses are normalized to 12 molybdenum atoms.

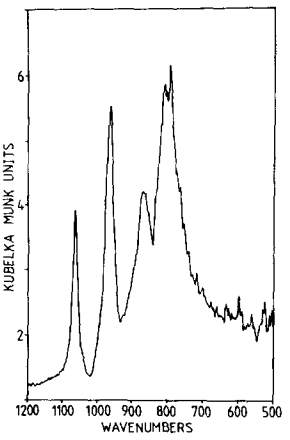

FIG. 15. Diffuse-reflectance IR spectrum of calcined (673 K) K_1. Wavenumber units are cm^{-1}.

DISCUSSION

Our characterization of the 12-molybdophosphate catalysts of formal composition $K_xH_{3-x}PMo_{12}O_{40} \cdot nH_2O$ as freshly prepared has shown that they are not single-phase materials, even as prepared, but are a multiphase mixture that is made more complex by calcination. Standard preparations give stoichiometric mixtures of the end members of the series,

$$(x/3)\ K_3PMo_{12}O_{40} + [(3 - x)/3]\ H_3PMo_{12}O_{40} \cdot nH_2O,$$

and calcination of mixtures containing the K_0 phase leads to the appearance of MoO_3 and other decomposition products.

The principal features of the catalysts of this series, as revealed by the experiments described above, are the following:

(1) The end member K_3 is a water-insoluble, neutral salt stable up to 920 K. It has a well-defined crystal structure and a ^{31}P solid-state NMR resonance at $\sigma = -4.3$ ppm. Any water physisorbed at 300 K is desorbed at 500 K. After calcination at 673 K for 5 h, the catalyst consists of well-formed, round or hexagonal crystallites 1–3 μm in diameter with clean surfaces containing $(PMo_{12}O_{40})^{3-}$ anions having the Keggin structure.

(2) The end member K_0 is a water-soluble Brønsted acid containing, as prepared, a variable concentration n of water of crystallization that tends to be inhomogeneously distributed throughout a given sample so as to give a poorly defined, multiphase crystal structure and multiple ^{31}P solid-state NMR signals that vary with n. The water of crystallization is released by 450 K; in the temperature interval $500 < T < 700$ K, constitutional water is released and some decomposition of the $(PMo_{12}O_{40})^{3-}$ anions occurs. One of the decomposition products is slightly reduced MoO_3, which has a characteristic Mo(V) ESR signal. Significantly, a cubic phase isostructural with the K_3 phase is also formed. In addition, at least two other intermediate decomposition products were identified. Whether the phase isostructural with K_3 is $(H_3O)_3PMo_{12}O_{40}$ was not established.

(3) No significant solid-solution range exists in freshly prepared mixed compositions K_x, $0 < x < 3$. In view of the different properties of the free acid K_0 and the neutral salt K_3, in particular their solubility in water, it is perhaps surprising that salts of intermediate composition obtained by the Tsigdinos method should ever have been assumed to be solid solutions. On the other hand, identification of a phase isostructural with K_3 among the products of a calcined K_0 phase is compatible with the existence of an epitaxial phase which, under the preparative conditions of a calcined mixed phase, could be stabilized as a surface coating on well-formed K_3 particles. Wetting of the surface of a K_3 particle by an epitaxial layer could be stabilized by H_3O^+ exchange with K^+ ions and/or proton transfer into n-type K_3 particles.

(4) After calcination, catalysts K_x ($0 < x < 2$) consist of small particles of K_3 formed into aggregates within a matrix of dehydrated K_0 and its decomposition products. The extent of decomposition of the K_0 phase depends upon x as well as upon the calcining time and temperature. Although the K_0-phase decomposition products may include a phase isostructural with K_3 that wets the K_3 particle surfaces, nevertheless the other decomposition products, including MoO_3, form a distinctly separate matrix. This dehydrated K_0 matrix not only inhibits K_3 particle growth, presumably by inhibiting K^+-ion diffusion, but it also provides interparticle interactions that produce aggregates of relatively large volume, thereby reducing the BET surface area of the catalyst. As demonstrated for K_1, these aggregates contain $PMo_{12}O_{40}$ units with the Keggin structure at their surface; these units provide a microsurface for interaction with adsorbed reactants. However, the K_0-phase decomposition products also present, including MoO_3, provide alternate catalytic surfaces where competitive interactions may occur.

(5) Catalysts K_x ($2 < x < 3$) have a morphology, after calcination, similar to that of K_3. A substantial fraction, which increases with x, of the K_0 phase (or one of its derivatives) is stable against calcination in this compositional range; the presence of MoO_3 is just detectable in calcined $K_{2.5}$. Moreover, a stable partial decomposition product of the K_0 phase appears to be isostructural with the K_3 phase and present on the K_3 particles as a K-deficient surface layer, as established by ESCA. Selected-area electron diffraction with HREM shows no streaking, indicating that the surface layers of the K_3 particles are isostructural with the bulk and are formed by an epitaxial

deposition. Identification of such an isostructural phase among the decomposition products of the calcined K_0 phase demonstrates the feasibility of forming an epitaxial surface layer on the K_3 particles. Such a surface layer, stabilized by K^+ and H_3O^+ on exchange across the interface and/or proton migration into an *n*-type K_3 phase, would permit K^+-ion diffusion through it and hence the growth of the bulk phase of the particles. The eventual morphology of the K_3 particles with such a surface layer would, in the absence of any significant concentration of other decomposition products, be similar to those found for the pure K_3 phase. The other decomposition products, such as MoO_3, can be expected to be present as mixtures having little intimate contact with the K_3/K_0 particles. On the other hand, such a surface layer would provide a Brønsted acidity not present at the surface of a pure K_3-phase particle, and this Brønsted acidity may influence significantly the performance of the catalyst.

(6) Catalysts K_x in the compositional range $2.5 \leq x \leq 3$ offer, after calcination, clean particles containing intact $PMo_{12}O_{40}$ Keggin structures on their surface, albeit with a varying degree of protonation of the $(PMo_{12}O_{40})^{3-}$ anion possible, ranging from zero to three protons. The concentration of other K_0-phase decomposition products is minimal. These catalysts therefore offer an ideal test-bed for mechanistic studies.

ACKNOWLEDGMENTS

We acknowledge the Science and Engineering Council for a Co-operative I.C.I.-Oxford University award and for financial support (P.L.G.). We also thank Mr. Neil Poole (I.C.I., Wilton) for helping with the diffuse-reflectance IR spectroscopy and Miss Wendy Flavell (Inorganic Chemistry Laboratory, Oxford) for assistance with the ESCA measurements.

REFERENCES

1. Pearce, R., and Patterson, W., "Catalysis and Chemical Processes," p. 279. Hill, London, 1981.
2. Clark, C. J., *Acta Crystallogr. B* **32,** 1545 (1976).
3. D'Amour, H., and Allman, R., *Z. Kristallogr.* **143,** 1 (1976).
4. Nakamura, O., Kodama, T., Ogino, I., and Miyaka, Y., *Chem. Lett.* **1,** 17 (1979).
5. Pope, M. T., *in* "Inorganic Chemistry Concepts," Vol. 8, p. 101. Springer-Verlag, Berlin/Heidelberg/New York/Tokyo, 1983.
6. Misono, M., Mizuno, N., Katamura, K., Kasai, A., Konishi, Y., Sakata, K., Okuhara, T., and Yoneda, Y., *Bull. Chem. Soc. Japan* **55,** 400 (1982).
7. Ai, M., *J. Catal.* **71,** 88 (1981).
8. Nakamura, S., and Ichihashi, H., "Proceedings, 7th International Congress on Catalysis, Tokyo, 1980," p. 755. Kodansha (Tokyo)/Elsevier (Amsterdam), 1981.
9. Ai, M., *J. Catal.* **85,** 324 (1984).
10. Tsigdinos, G. A., *Ind. Eng. Chem. Res. Dev.* **13,** 267 (1974).
11. Akimoto, M., Tsuchida, Y., Sato, K., and Echigoya, E., *J. Catal.* **72,** 83 (1981).
12. Konishi, Y., Sakata, K., Misono, M., and Yoneda, Y., *J. Catal.* **77,** 169 (1982).
13. Boeyens, J. C. A., McDougal, G. J., and van R. Smit, J., *J. Solid State Chem.* **18,** 191 (1976).
14. Serwicka, E., *J. Solid State Chem.* **51,** 300, (1984).
15. McMonagle, J. B., and Moffat, J. B., *J. Colloid Interface Sci.* **101,** 479 (1984).
16. Rocchiccioli-Deltcheff, C., Thouvenot, R., and Franck, R., *Spectrochim. Acta A* **32,** 587 (1976).